Langmuir

Article

pubs.acs.org/Langmuir

Adhesion Mechanisms of the Contact Interface of TiO_2 Nanoparticles in Films and Aggregates

S. Salameh,[†] J. Schneider,[‡] Jens Laube,[‡] A. Alessandrini,[§,#] P. Facci,[§] J. W. Seo,[∥] L. Colombi Ciacchi,*[,‡,⊥] and L. Mädler*[,†]

[†]Foundation Institute of Materials Science (IWT), Department of Production Engineering, University of Bremen, Bremen, Germany

[‡]Hybrid Materials Interfaces Group, Department of Production Engineering and Bremen Center for Computational Materials Science, University of Bremen, Bremen, Germany

[§]Institute of Nanoscience, National Research Council (CNR), Modena, Italy

[∥]Department of Metallurgy and Materials Engineering, KU Leuven, Leuven, Belgium

[⊥]Fraunhofer Institute for Manufacturing Technology and Advanced Materials IFAM, Bremen, Germany

[#]Department of Physics, University of Modena and Reggio Emilia, Modena, Italy

ABSTRACT: Fundamental knowledge about the mechanisms of adhesion between oxide particles with diameters of few nanometers is impeded by the difficulties associated with direct measurements of contact forces at such a small size scale. Here we develop a strategy based on AFM force spectroscopy combined with all-atom molecular dynamics simulations to quantify and explain the nature of the contact forces between 10 nm small TiO_2 nanoparticles. The method is based on the statistical analysis of the force peaks measured in repeated approaching/retracting loops of an AFM cantilever into a film of nanoparticle agglomerates and relies on the in-situ imaging of the film stretching behavior in an AFM/TEM setup. Sliding and rolling events first lead to local rearrangements in the film structure when subjected to tensile load, prior to its final rupture caused by the reversible detaching of individual nanoparticles. The associated contact force of about 2.5 nN is in quantitative agreement with the results of molecular dynamics simulations of the particle−particle detachment. We reveal that the contact forces are dominated by the structure of water layers adsorbed on the particles' surfaces at ambient conditions. This leads to nonmonotonous force−displacement curves that can be explained only in part by classical capillary effects and highlights the importance of considering explicitly the molecular nature of the adsorbates.

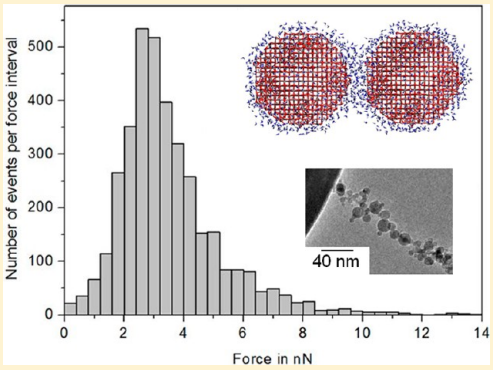

1. INTRODUCTION

Adhesion forces between nanoparticles play a major role in unit operations such as fluidization,[1] agglomeration, and coating.[2] These processes are utilized in a wide range of technical fields, including the production of pharmaceutical powders,[2] paints,[3] and solar cells.[4] Currently, particle−particle adhesion is interpreted in terms of continuum models that are able to take into account the effects of humidity (capillary forces)[5−7] surface roughness and electrostatics (e.g., within DLVO-like theories)[8,9] and hold especially for particle sizes in the micrometer range. However, for smaller particles with characteristic sizes of the order of 10 nm, more subtle effects beyond continuum theories, such as the molecular structure of adsorbate layers or the distribution of terminal groups on the particles' surfaces are likely to influence and even dominate the adhesion behavior.[10,11] The investigation of such effects is nontrivial and calls for a combination of accurate measurements with atomistic simulations, as performed in the present work.

Adhesion forces between micro- and nanoparticles can be directly quantified with force spectroscopy measurements using an atomic force microscope (AFM),[12] as performed for instance by Larson et al.[13] after functionalizing the AFM tips with single microparticles. However, the tip functionalization becomes increasingly difficult with decreasing particle size. Ong and Sokolov[14] have presented a method to attach ceria (CeO_2) nanoparticles (50 nm) on an AFM tip with epoxy glue. They used these functionalized tips to measure the adhesion force between the nanoparticles and a flat silica surface. A chemical method was used by Vakarelski et al.[15] to place single gold nanoparticles (20−40 nm) on the tip of an AFM cantilever to measure the adhesion force between nanoparticles and mica. In another study, the adhesion forces between variously shaped AFM tips and a film of TiO_2 nanoparticles have been measured as a function of the environmental relative humidity and interpreted with capillary theories.[5] Gluing a colloid on a tipless cantilever and measuring the adhesion force against a film of

Received: June 1, 2012
Revised: July 10, 2012
Published: July 11, 2012

nanoparticles (50−180 nm) is a common variation of using the pure tip.[16] Notably, in all these studies no nanoparticle−nanoparticle interactions were measured directly.

A further difficulty arises from the fact that nanoparticles within unit operations often cluster together in aggregates via hard (chemical) bonds, and the aggregates in turn form agglomerates as a consequence of weak (physical) bonds between the primary particles forming the aggregates.[17] Therefore, it is not trivial to isolate single particles as instead routinely performed for the case of larger colloids. Adhesion forces of the order of 1 nN have been measured between graphitic nanoparticle chain aggregates by repeated approaching and retracting of a nonfunctionalized AFM tip into an aggregate film.[18] The force distribution corresponding to ∼1000 of these force measurements presented three maxima that were related to sliding, rolling, and detaching events between the aggregates. In a further work, the force required to separate covalently bonded primary particles in aggregates was measured by means of a combined AFM/SEM setup and found to be one magnitude higher than the one required for detaching two aggregates.[17] Interestingly, the adopted technique allowed imaging the stretching process of the aggregates in situ during the force spectroscopy experiments.

In this paper, we investigate the adhesion mechanisms of TiO_2 nanoparticle aggregates in porous films using a combination of AFM force spectroscopy, in-situ AFM/TEM, and all-atom molecular dynamics (MD) techniques. This enables us to (i) measure directly the particle−particle contact forces, (ii) visualize the behavior of the aggregates during stretching of the film up to the final particle−particle detachment events on the nanometer scale, and (iii) interpret the obtained results on the basis of atomistic simulations that help revealing the nature of the particle−particle contacts at atmospheric conditions. In particular, linking the experimental and simulation results allows us to elucidate the microscopic mechanisms underlying the adhesion of nanoparticles. While previous simulation studies have been reported e.g. for the contact and sintering of dry TiO_2 nanocrystals,[19,20] we take into account the effects of adsorbed water molecules,[21,22] which largely influence the adhesion forces under atmospheric conditions.

2. METHODS

Particle Synthesis. A flame spray reactor was used to produce TiO_2 nanoparticle films on a mica substrate by the FSP method.[23] The liquid precursor consisted of 0.5 molar Ti(IV) isopropoxide (Sigma-Aldrich, 99.9% purity) in xylene. The precursor was fed with the help of a syringe pump AJ-5803 (Angel) at a constant rate of 5 mL/min through a capillary of a two-phase-mixing nozzle. The precursor was dispersed into fine droplets by a 1.5 bar stream of O_2 (5 L/min), surrounded by a methane/oxygen flow (1.5 L/min/3.2 L/min) in order to stabilize the flame. All gas flow rates were controlled with mass flow controllers from Bronkhorst. The produced aggregates were deposited on a 1 cm^2 mica substrate (Science Service) secured to a water-cooled holder 25 cm above the nozzle. At the same time, particles were collected on a GF6 glass fiber filter (Whatman) 60 cm above the nozzle. The spraying time for the film was 2 min according to the theory of FSP-synthesized film growth.[24] For AFM manipulation inside the TEM particles were sprayed on the edge of a tungsten wire with 0.3 mm diameter. The spraying time for the wire was 2 s because thicker films showed instabilities during the experiments inside the TEM, in particular upon exposure to the electron beam.

Particle Characterization. Nanoparticles were characterized with X-ray diffraction (XRD) using a PANalytic X'Pert MDP Pro. The measurements were taken from 0° to 140° using a scan speed of 1.34°/min per 0.0334°. Crystalline phases were determined using the BRASS 2.0 software.[25] The specific surface area was measured using nitrogen adsorption−desorption measurements on Nova 3000e (Quantachrome). The specific surface area (SSA) was derived using the theory based on Brunauer−Emmett−Teller (BET) adsorption. SSA was used to calculate the primary particle size. Imaging of the nanoparticle aggregate films was performed using a scanning electron microscope Nova NanoLab 200 from FEI. The particle surface was investigated by TGA using an STA 449 F3 Jupiter from Netzsch.

Force Measurements. The adhesion forces between nanoparticle aggregates were measured with an atomic force microscope (Multimode from Bruker) in air at room temperature at a constant relative humidity of 50%. Force measurements were performed with a Si_3N_4 cantilever (DNP-10 from Bruker/spring constant = 0.12 N/m) in force volume mode, a vertical cantilever speed of 5.06 μm/s, 32 × 32 measurement points, and a scan size of 500 nm^2. Being interested in the various different phenomena that take place in particle chains during extension and detachment, the indentation value was chosen in order to avoid too deep penetration of the tip into the film, thus enabling the observation of specific chain stretching events.

In order to ensure constant conditions, all 1024 force measurements were made consecutively within 1 h, using the same cantilever in the lab environment. The cantilever was afterward checked using the SEM to exclude tip damaging during the measurements. The AFM was mounted on a vibration-isolated table. The force curves were analyzed following Farshchi-Tabrizi et al.[5] using the R-cran software, version 2.13. The analysis took into account the slope of the baseline, subtracting its value from those of the peak forces.

The in-situ AFM/TEM investigations were done inside a Philips CM 200 FEG transmission electron microscope (column vacuum around 10^{-6} mbar), using a conducting AFM/TEM holder from the Nanofactory Instruments AB. In these experiments a Si_3N_4 cantilever with a spring constant of k = 5.3 N/m was used.

Molecular Dynamics Simulations. The molecular dynamics (MD) simulations were carried out using the LAMMPS[26] program package at 300 K constant temperature with an integration time step of 2 fs. The interactions within the oxide crystal were described by a slightly modified implementation[27] of the force field of Matsui and Akaogi;[28] the surface water interactions were modeled by the potential developed by Schneider et al.[29] for TIP3P[30] water molecules. In this approach, we assume that the true interactions at the TiO_2/water interface can be mapped onto a combination of van der Waals and Coulomb forces, which may be a source of systematic errors for the case of complex systems. We note, however, that our potential gives a quantitatively accurate estimate of the heat of hydration of rutile crystals compared with available experimental results (see ref 25). The particle models were created by carving a sphere of 4 nm diameter out of rutile or anatase single crystals. In order to heal initial surface defects, the particles were annealed and structurally relaxed. The particles' surfaces were hydrated first by adding an OH terminal group to each Ti surface atom coordinated by less than five O atoms and an H atom to the nearest undercoordinated surface O atom. Afterward, they were equilibrated in bulk water, leading both to water chemisorption (direct Ti−O bonds) on exposed Ti atoms and physisorption via hydrogen bonds to surface terminal groups. The final, partially hydroxylated particle models surrounded by adsorbed water were obtained upon removing all physisorbed water molecules beyond the desired number (11 molecules per nm^2 in accordance with the TGA experiments).

Force−displacement curves between hydrated particles were obtained in a series of MD simulations, in which two particles were constrained to a certain center-of-mass separation and the atoms belonging to the oxide crystals were not allowed to move. For a given separation distance, at each MD step the interparticle force was calculated as the sum of all individual forces acting on the atoms of one oxide crystal. The resulting values were averaged over a 2 ns simulation following an initial equilibration period of 0.5 ns, which was discarded from the analysis. This ensured convergence of the computed contact

force at each separation distance, taking into account the equilibrium structure of water molecules surrounding the two particles.

3. RESULTS AND DISCUSSION

3.1. Force Spectroscopy Measurements. We start our investigation with the FSP deposition of an 8 μm thick, highly porous film of TiO_2 nanoparticle aggregates on a flat mica substrate (see SEM image in Figure 1). As revealed by XRD

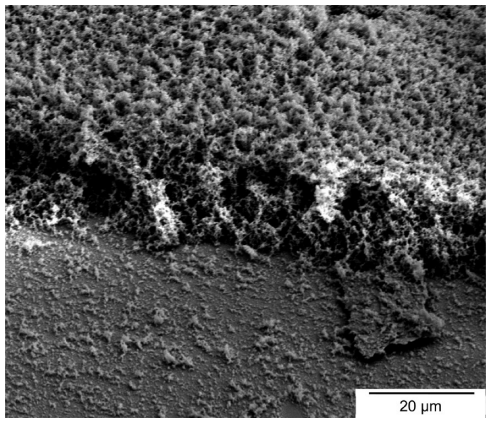

Figure 1. SEM picture of a film of TiO_2 aggregates after 2 min deposition time. The thickness of the film in the upper half is 8 μm. This layer has a very high porosity (~98%). The lower part consists of a monolayer of TiO_2 aggregates and agglomerates.

analysis, the synthesized material is mainly in the anatase phase with a primary particle size of d_{BET} =12 nm, as measured by nitrogen adsorption. The porosity of the film is 98%.[24] The bottom half in Figure 1 shows a thin layer of rather separate TiO_2 aggregates at the outer film boundary, in the area where the mica substrate was fixed into the holder.

The film shown in Figure 1 is then used to investigate the adhesion between nanoparticle aggregates by means of AFM force spectroscopy. To this aim, we acquire a set of sequential 1024 force–displacement curves by repeatedly approaching an AFM tip to the film up to contact with the film's top surface and retracting up to full detachment. This procedure results in the progressive transfer of aggregates from the film to the tip, which is clearly visible in characteristic SEM tip inspections after 10, 50, and 1000 approach/retraction events (Figure 2(I), A, B, and C, respectively). The analysis thus reveals strong adhesion between the aggregates and the AFM tip, which has also been reported in the literature for the case of a silicon tip and TiO_2 nanoparticles.[5]

Importantly, the SEM tip imaging shows that both the edge and the sides of the tip become decorated with multiple aggregates. As the experiment proceeds, more and more aggregates attach forming agglomerate structures with extended branches (Figure 2(I)). It is thus expected that multiple aggregates bound to the tip get in contact with the underlying film during each tip approach and subsequently break during each tip retraction. The situation is schematically depicted in Figure 2(II)A,B for the initial stages of the experiment (a single chain of aggregates is stretched between the tip and the film) and Figure 2(II)C,D for a later stage (where several aggregates can be stretched at the same time). In fact, during the retraction of the tip, the agglomerates unfold and detach leading to multiple peaks in each measured force–distance curve (Figure 3).

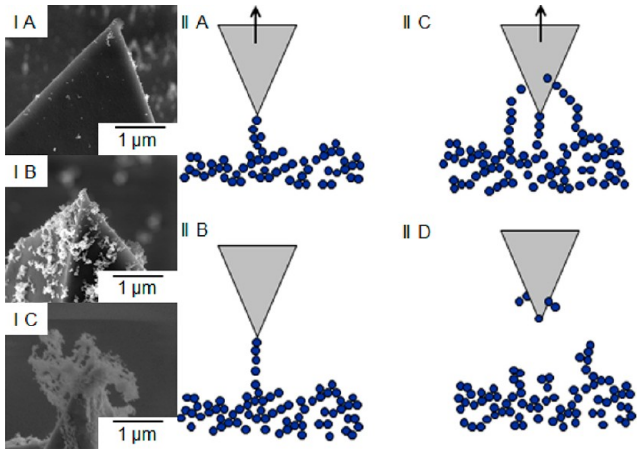

Figure 2. (I) Three AFM tips after probing the TiO_2 film. (II) Two different scenarios (A + B and C + D) of the agglomerate behavior during retraction of the tip.

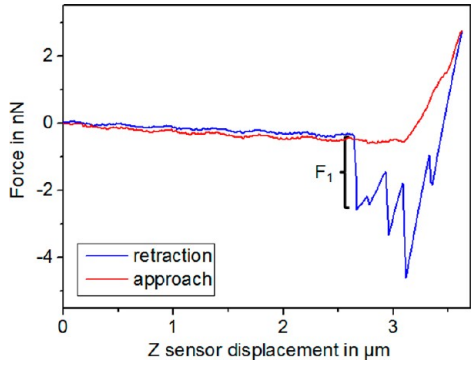

Figure 3. A force–distance curve of detaching TiO_2 nanoparticle aggregates. The peaks are supposed to be related to sliding, rolling, and detachment events. Visible oscillations in the noncontact portion of the curve are due to laser interferences.

A statistical distribution of a total of 3677 peaks for the 1024 force–displacement curves collected in a single experiment is shown in Figure 4. These values correspond to the differences between each peak and the zero line recorded at atmospheric pressure and 50% relative humidity. The monomodal histogram shape can be fitted to a log-normal distribution function with a median of 3.1 nN and a geometric standard deviation (gsd) of 1.7. The maximum of the density distribution is at 2.5 nN.

In order to investigate the effect of the increasing tip decoration with aggregates during the course of the experiment, we include in the inset of Figure 4 a time-dependent analysis of the force distributions obtained within four consecutive intervals of 256 measurements. The median values are roughly constant at 2.9 nN in the first three measurement intervals and increase to 4 nN only for the last 256 measurements. The gsd, instead, increases steadily with increasing number of performed measurements. This latter finding is consistent with an increasing number of aggregates transferred from the film to the AFM tip (see Figure 2(I)) and thus with a correspondingly increased force in agglomerate rearrangement based on stronger agglomerates between the tip and the film, contributing to the spreading of the force-peak distribution. However, the fact that the maximum and the median of the distribution remain nearly constant up to the final stage of the experiment suggests the presence of a fundamental decohesion

dx.doi.org/10.1021/la302242s | Langmuir 2012, 28, 11457–11464

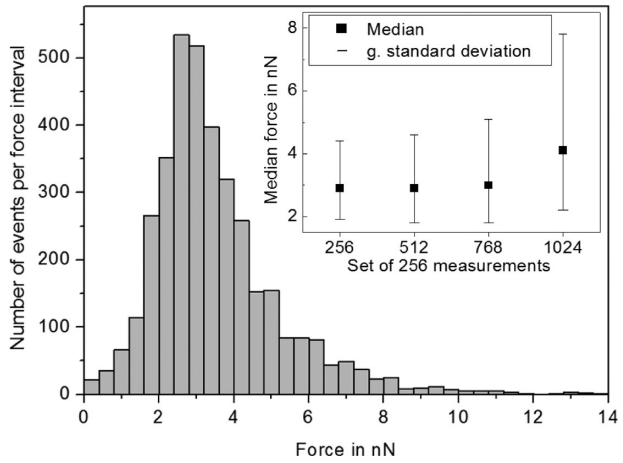

Figure 4. Force-peak histogram analysis of 1024 force−displacement curves collected on the TiO_2 film. In the inset the median and geometric standard deviation for consecutive sets of 256 measurements are shown. The increase of the median for the last point is most probably related to the increased number of aggregates on the tip (see Figure 2(I)).

process with a well-defined associated force during the tip retraction. Whether this process can be interpreted as the detachment of two primary particles in the film is the subject of the following two Sections.

3.2. In-Situ AFM/TEM Imaging. The change of the agglomerate structure during approach and retraction of an AFM tip is investigated in real time and recorded in situ using the combined AFM-TEM setup described in the Methods section. Here, a tungsten wire is coated with TiO_2 nanoparticle aggregates for the force measurements (Figure 5(I)A+B). Unfortunately, the force sensitivity of the instruments used is limited to about 10−20 nN, thus preventing a simultaneous measurement of the resulting adhesion forces as in the previous section. However, we are able to image with a high spatial resolution each primary particle of the agglomerate bridging the AFM tip with an underlying nanoparticle film after the approach and follow the evolution of the agglomerate structure during the tip withdrawal.

Figure 5(II)A−F shows a time series of movie frames recorded while stretching a TiO_2 agglomerate (consisting of multiple nanoparticle aggregates) over a distance of 150 nm. The AFM tip is in the upper corner of each picture; the nanoparticle film is in the lower right corner. During pulling the agglomerate over 150 nm, the increasingly applied force stretches the agglomerate while single aggregates rearrange by means of sliding or rolling mechanisms which lead to the unfolding of kinks (Figure 5(II)B,C). The process is reminiscent of the unfolding of tertiary structure elements of proteins in similar AFM force spectroscopy experiments.[31] Eventually, this leads to a stretched agglomerate where single nanoparticle aggregates are aligned next to each other in a roughly linear chain (Figure 5(II)D) before its sudden rupture, clearly associated with the detachment of a primary particle-to-particle contact.

Approaching the detached agglomerates again leads to their reconnection (Figure 5(II)F), indicative of reversible rupture events dominated by weak (nonchemical) forces. Notably, the reconnection does not occur at the same point where the agglomerate had detached, and stretching the agglomerate again shows a different detachment point. By repeating the experiment many times, we observe that the detachment point tends to move farther and farther away from the tip, which agrees with the process of progressive transfer of larger and larger aggregates observed in SEM tip inspection images (see Figure 2(I)A−C).

3.3. Analysis of the Statistical Distribution of Adhesion Forces. The in-situ AFM/TEM investigations show that the stretching of agglomerates bridging the AFM tip with the underlying nanoparticle film leads to (i) an initial rearrangement of the agglomerate structure (unfolding) until formation of a roughly linear chain of aggregates and eventually (ii) the rupture of such chain after breaking of single particle−particle contacts. It should be considered that measurements in vacuum could change the contact behavior of the aggregates compared to atmosphere conditions. Especially the amount of adsorbed water molecules is expected to be reduced, although not completely, since desorption of chemisorbed water molecules only takes place at temperatures of the order of 400 K.[32] Therefore, we do not expect a dramatically different mechanism of adhesion to take place in vacuum or in air.

Furthermore, the very stiff cantilever used in the in-situ TEM measurements changes the loading rate compared to the measurements performed by AFM force spectroscopy, which

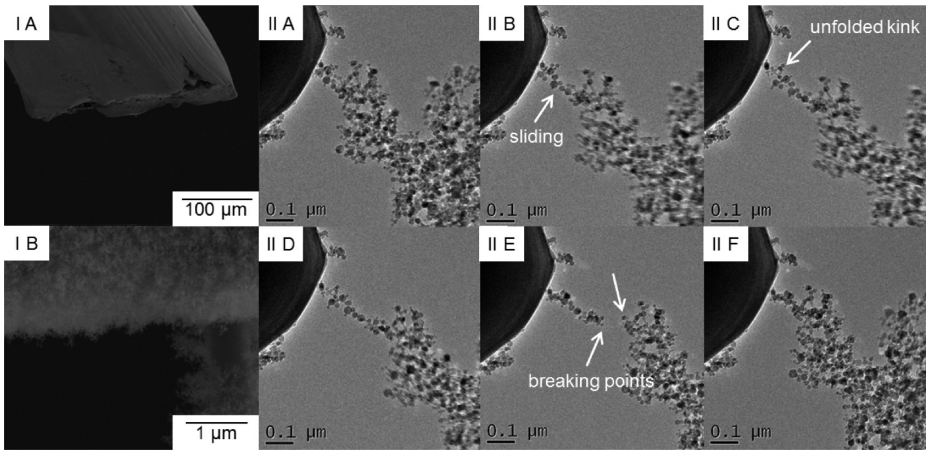

Figure 5. AFM-TEM experiments: (I)A, tungsten wire; (I)B, TiO_2 nanoparticle agglomerates deposited in situ with FSP on a 0.3 mm tungsten wire; (II)A−F selected frames (in time series) from a movie recorded during one AFM approach and retraction (time span: 5 s).

dx.doi.org/10.1021/la302242s | *Langmuir* 2012, 28, 11457−11464

could affect the unfolding pathway of the agglomerates. Qualitatively, however, the observed unfolding and rupture processes in the TEM (Figure 5) agree well with the unfolding process suggested by the sawtooth curves measured with the AFM (Figure 3). Therefore, it is very likely that the vacuum does not remove all water molecules, and the qualitative contact behavior is not altered significantly.

In particular, the final rupture event is the one that causes the force−displacement curve to jump back to the baseline of zero force in each approach/reproach cycle with a sudden step (labeled as F_1 in Figure 3). The distribution of forces representative for only this last step is shown in Figure 6.

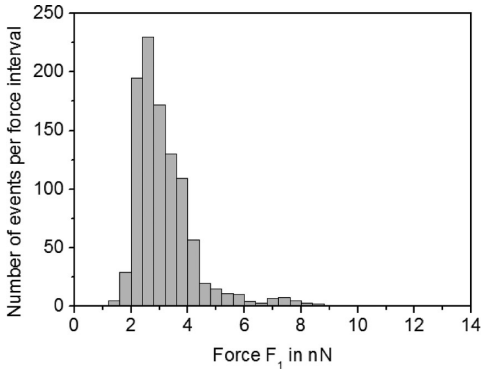

Figure 6. Force histogram of the last peak of TiO_2 force−displacement curves (F_1), most likely related to the primary particle−particle contact (see AFM-TEM studies). The detaching force is at least 1.2 nN and most frequently 2.5 nN. The few number of higher forces is probably due to detaching of aggregates at multiple contact points.

The histogram presents a log-normal distribution with a maximum at 2.5 nN. Forces lower than 1.2−1.6 nN are absent from the histogram, indicating a minimum threshold in the contact force between two nanoparticles. Moreover, the maximum of the distribution coincides with the maximum of the global distribution in Figure 4. We therefore conclude that the characteristic value of contact force between two of the TiO_2 nanoparticles in our sample at atmospheric conditions is about 2.5 nN. The small number of higher forces (small subpeak at 7.5 nN in the distribution of Figure 4) is probably due to the detachment of aggregates bridged by multiple contacts. These multiple contacts are probably also the cause of the increased gsd in Figure 4. Here the increasing number of cumulated aggregates on the tip increases the likelihood of such multiple contacts.

Indirectly, the difference between the two distributions in Figures 4 and 6, together with the in-situ TEM imaging of the stretching event, suggests that the forces smaller than 1.2 nN present in the global distribution may be associated with sliding or rolling of the aggregates leading to unfolding of the strained agglomerates. We expect each rearrangement of the agglomerate structure prior to its final rupture, be it due to unfolding or to temporary detachment of two primary particles, to be associated with a jump in the measured force−distance curves. The distribution of these jumps, namely of the differences between each maximum and the following minimum in the force−displacement curve, is reported in Figure 7. This distribution once again presents a maximum centered at the force value required to detach two primary particles (~2.5 nN). However, it also presents a secondary maximum at lower forces (~0.6 nN), which is representative of other rearrangement

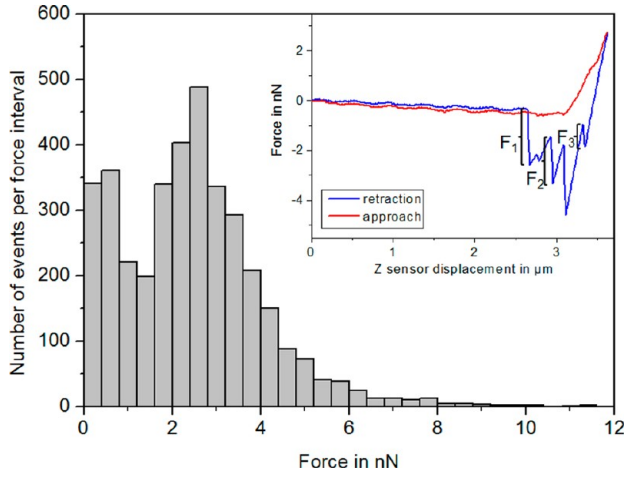

Figure 7. Histogram distribution of the differences between maxima and minima in the sawtooth-shaped force−displacement curves (see inset).

process such as for instance sliding and rolling of the nanoparticle aggregate on each other.

3.4. Molecular Dynamics Modeling. The experimental investigations indicate that a clear characteristic force of about 2.5 nN characterizes the contact between our TiO_2 nanoparticles at atmospheric conditions, that is, at room temperature and at a relative humidity within 40−50%. Under these conditions, a thin layer of water molecules (both chemisorbed and physisorbed) is expected to be present on the particle surface. Indeed, the contact forces between oxide particles are often interpreted in terms of capillary effects, which often dominate over other interactions, for instance of the van der Waals type.[5]

In this section we aim at rationalizing our results and search for the dominating interactions responsible for the particle−particle contacts in the case of our TiO_2 aggregates. These present primary particle sizes in the order of 10 nm or smaller, at which the continuum theories at the basis of classical capillary effects may become questionable. We therefore perform all-atom molecular dynamics (MD) simulations of the detachment of two crystalline TiO_2 particles (in the rutile or anatase phase) of spherical shape, terminated with chemisorbed OH and H_2O groups and surrounded by a number of physisorbed H_2O molecules.

The amount of adsorbed water under our experimental conditions is determined by means of TGA measurements where the TiO_2 nanoparticle aggregates are heated up to 700 °C, and the mass decrease due to removed water is measured. We obtain an average of about 11 water molecules per nm^2 on the surface of the nanoparticles. Accordingly, we construct a particle model including 11 water molecules per nm^2. The diameter of the particle is chosen to be 4 nm, which is smaller than the characteristic particle size investigated experimentally but keeps the computational efforts within reasonable limits and allows us to compute the force−displacement curves with good statistical accuracy (see Methods for computational details).

Representative force−displacement curves are shown in Figure 8. Importantly, no qualitative differences in the overall force−displacement behavior are found for the two polymorphs investigated (anatase and rutile).

dx.doi.org/10.1021/la302242s | Langmuir 2012, 28, 11457−11464

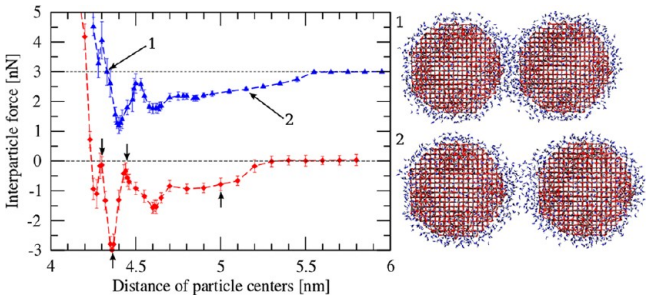

Figure 8. Computed force–distance curves for anatase (blue) and rutile (red) TiO_2 nanoparticles bearing a water coverage of 11 molecules/nm^2, as obtained from constrained MD simulations, along with two representative snapshots corresponding to contact at equilibrium (1) and attraction due to a capillary water neck (2). The small arrows mark four selected distance points for the analysis of the water structure between the particles (shown in Figure 9). The forces between anatase particles are shifted by +3 nN for clarity.

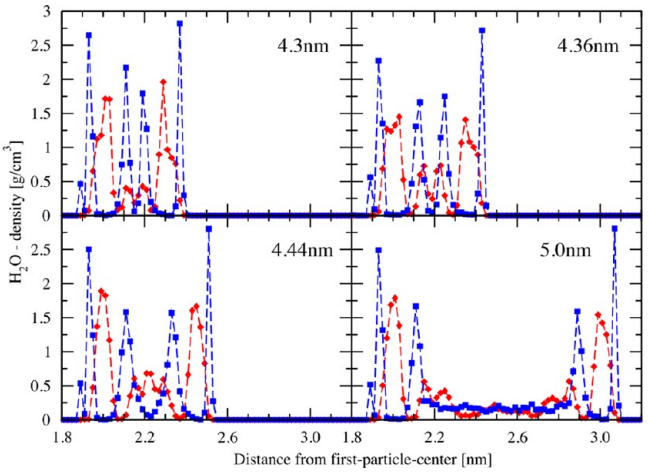

Figure 9. Analysis of the density of water molecules in the region of the particle–particle contact, along the z direction connecting the particle centers, at different separation distances (small arrows in Figure 8). The blue and red curves refer to the density of the H and O atoms, rescaled to the density of bulk liquid water. The analysis refers to rutile particles, which show better-resolved peaks in the mutual particle orientation chosen here.

When the two particles start approaching, at a center-to-center distance of about 5.5 nm a first water neck builds up between them, leading to an attraction force that increases roughly linearly up to a value of ~1 nN at a separation of about 4.8 nm, as expected from a classical capillary effect. (The small difference in the onset of attraction for the two curves is due to different random fluctuations of the physisorbed molecules prior to formation of a capillary neck in the two individual simulations and is not to be considered as a material-dependent feature.) At shorter distances, however, the force profile features pronounced oscillations, which can be associated with interactions between the structured water layers above the particle surfaces (see below). Maximum adhesion forces of about 2 and 3 nN at center-of-mass distances of 4.4 and 4.35 Å are computed for rutile and anatase, respectively. These values agree well with the AFM force spectroscopy measurements. An analysis of the individual contributions to the total force shows that the bare oxide–oxide interactions become relevant only at separation smaller than the computed equilibrium distance, whereas the major contribution to the maximum cohesion force is due to the water–water interactions between the adsorbed molecules.

In order to clarify the effect of the water structure between the particles on the measured force, we plot the densities of O and H atoms belonging to both chemisorbed and physisorbed water molecules along the direction connecting the centers of mass of the two particles, for selected separation distances (Figure 9). At the equilibrium distance of 4.3 nm, the O density shows two outer maxima corresponding to chemisorbed water molecules (at 1.9 and 2.4 nm) and two inner maxima (at 2.1 and 2.2 Å) corresponding to the physisorbed water present between the particles. The H density distribution also present four correspondent peaks. The inner ones are in correspondence with the inner O peaks, indicating, on average, a flat arrangement of physisorbed water. The outer H peaks, instead, are at distances further off the particle centers than the corresponding O peaks, consistently with the preferentially upright binding mode of chemisorbed H_2O.[29]

After pulling the particles apart, a first force is experienced because of the stretching of the water layer structure off the equilibrium (see Figure 9, top right panel at the separation of 4.36 nm). This effect is responsible for the maximum adhesion force visible in the force–displacement curves. At a larger separation of 4.44 nm, the two layers are entirely separated, and the water molecules reorient to an upright configuration, as visible by the appearance of a new, small central H peak at 2.2 nm. This configuration corresponds to a strong decrease of the adhesion force up to almost the baseline. At larger and larger separation, new water molecules are able to diffuse in the region between the particles forming the capillary neck, with a correspondent increase of the O density in the central region and leveling of the adhesion force to the initial value of about 1 nN.

4. CONCLUSIONS

In summary, our investigations show that the contact forces between individual particle aggregates in agglomerate films are dominated by the layers of adsorbed water present on the particles' surfaces at ambient conditions. Differently from the case of classical capillary theories, the force–displacement curves obtained in accurate, all-atom molecular dynamics modeling present marked oscillations arising from the structural arrangement of water molecules in surface proximity. Indeed, the maximum adhesion force is 2–3 times larger than the one resulting from the formation of a capillary water neck between the particles (see Figure 8). Future studies shall be devoted to investigate the precise dependency of the adhesion forces on the ambient humidity (that is, on the amount of physisorbed water molecules) and on the particle size. These investigations could help to understand the dispersion of TiO_2 aggregates in various environments, including liquids, and the effect of capping agents controlling the interactions. Results in many topics like e.g. nanobio interactions depend strongly on the dispersion of the nanoparticles. Since the dispersion behavior changes from study to study, it is difficult to create reliable and reproducible data.[33−36] Therefore, a deeper understanding of the fundamental nanoparticle interactions could help to create standardized tests for nanoparticle aggregates in many important contexts, including in particular nanotoxicology assessments.

Importantly, we have demonstrated that precise experimental information about the characteristic adhesion forces between individual particles can also be obtained experimentally, by

dx.doi.org/10.1021/la302242s | Langmuir 2012, 28, 11457−11464

means of AFM force spectroscopy performed on freshly deposited particle films directly after flame spray pyrolysis synthesis. The strategy employed here, namely of repeated approaching/retracting loops of an AFM tip into the film, is capable of sensing primary particle/particle contact forces without specific functionalization of the tips with individual particles, which would be exceedingly difficult for particle sizes of few nanometers.

The statistical analysis of the peak force distributions, combined with the TEM visualization of the film stretching behavior, clearly highlight a characteristic decohesion event associated with a force of 2.5 nN, which is in the range of the forces obtained by MD modeling. We should note that an exact quantitative agreement would require a more complex analysis of the mechanical response of the entire film. In particular, it is not clear at the present stage how to correlate the size distribution of the nanoparticles in the film with the "weakest link" of the stretched chains (see Figure 5(II)), which gives rise to the measured rupture forces ("F1" distribution in Figure 6). The TEM imaging reveals that it is the contact between the smallest particles in each stretched chain that breaks first. Therefore, our experiments most likely give information about the contact forces between particles smaller than the average particle size in the film (in our case, 10 nm). This would explain why the force values computed in our MD simulations, which are performed with particles of only 4 nm size, are very similar to the values obtained experimentally (about 2.5 nN in both cases). We also note that a more thorough MD study of the variation of the computed forces due to different mutual orientations of the two particle crystals shall be performed in further works. In particular, it is the mutual orientation, together with the particle radius, that define the precise structure of the water layers shared by the two particles in the contact point and thus the absolute values both of the maximum adhesion force and of the capillary contribution. Finally, small variations of the interaction potential parameters, especially of the atomic point charges, may also influence the agreement between simulations and experiments.

In addition to the final rupture forces, the AFM force peak distributions during the stretching of aggregate chains also contain contributions due to particle rearrangement events such as sliding or rolling. Some of these events are characterized by forces of the order of 0.5 nN (that is, significantly smaller than the stretching/decohesion forces, as visible in the bimodal distribution in Figure 7). However, rolling, sliding, stretching, and other concerted rearrangements of the films are hard to distinguish with sufficient clarity without a more thorough and quantitative analysis of the AFM/TEM stretching experiments and corresponding MD simulations including shear forces between nanoparticles in contact.

As a note of caution, we would like to stress here that the different conditions between the AFM force measurements (in humid air) and the in-situ AFM/TEM imaging (in vacuo) could in principle lead to very different adhesion mechanisms between the particles. We think that this is unlikely, since complete removal of the adsorbed water in vacuo would require heating up to about 400 K.[32] However, this issue shall be investigated carefully in future studies aiming to quantify the adhesion forces under vacuum conditions.

In summary, our work defines an approach based on combined AFM force spectroscopy and MD simulations to investigate the water-mediated contact forces between individual nanoparticles in the size range of few nanometers. This approach shall be used in future investigations to elucidate (i) the scaling laws underlying the dependencies of the contact forces on humidity and particle-size beyond classical capillary theories, (ii) the physical nature and absolute values of the forces associated with rolling, sliding and stretching events between single particles, and (iii) the overall mechanical response of agglomerate films of nanoparticles subjected to external loads, which are of high importance for unit operations in nanoparticle processes and applications. These investigations are also expected to foster a deeper understanding of the nanoparticles behavior and fate in complex environments such as for instance physiological conditions.

AUTHOR INFORMATION

Corresponding Author

*E-mail: colombi@hmi.uni-bremen.de (L.C.C.), lmaedler@iwt.uni-bremen.de (L.M.).

Notes

The authors declare no competing financial interest.

ACKNOWLEDGMENTS

We thank Deutsche Forschungsgemeinschaft (DFG) for funding this project within the priority program "Partikel im Kontakt – Mikromechanik, Mikroprozessdynamik und Partikelkollektive" (SPP 1486) under grants MA 3333/3 and CO 1043/3. Support from the State of Bremen under the initiative "Func-Band" and from the EU-FP7-NMP grant 229205 "ADGLASS" is also acknowledged. We also thank Sabine Leroch (Universität für Bodenkultur, Wien) and Uri Sivan (Technion Haifa) for fruitful discussions and the group of A. Rosenauer (University of Bremen) for the SEM investigations.

REFERENCES

(1) Nam, C. H.; Pfeffer, R.; Dave, R. N.; Sundaresan, S. Aerated vibrofluidization of silica nanoparticles. *AIChE J.* **2004**, *50*, 1776–1785.

(2) Jono, K.; Ichikawa, H.; Miyamoto, M.; Fukumori, Y. A review of particulate design for pharmaceutical powders and their production by spouted bed coating. *Powder Technol.* **2000**, *113*, 269–277.

(3) Kumar, A.; Vemula, P. K.; Ajayan, P. M.; John, G. Silver-nanoparticle-embedded antimicrobial paints based on vegetable oil. *Nat. Mater.* **2008**, *7*, 236–241.

(4) O'Regan, B.; Gratzel, M. A low-cost, high-efficiency solar cell based on dye-sensitized colloidal TiO_2 films. *Nature* **1991**, *353*, 737–740.

(5) Farshchi-Tabrizi, M.; Kappl, M.; Cheng, Y. J.; Gutmann, J.; Butt, H. J. On the adhesion between fine particles and nanocontacts: An atomic force microscope study. *Langmuir* **2006**, *22*, 2171–2184.

(6) Butt, H.-J.; Farshchi-Tabrizi, M.; Kappl, M. Using capillary forces to determine the geometry of nanocontacts. *J. Appl. Phys.* **2006**, *100*, 024312.

(7) Ebenstein, Y.; Nahum, E.; Banin, U. Tapping mode atomic force microscopy for nanoparticle sizing: Tip-sample interaction effects. *Nano Lett.* **2002**, *2*, 945–950.

(8) Derjaguin, B.; Landau, L. Theory of the stability of strongly charged lyophobic sols and of the adhesion of strongly charged particles in solutions of electrolytes. *Prog. Surf. Sci.* **1993**, *43*, 30–59.

(9) Phenrat, T.; Saleh, N.; Sirk, K.; Tilton, R. D.; Lowry, G. V. Aggregation and sedimentation of aqueous nanoscale zerovalent iron dispersions. *Environ. Sci. Technol.* **2007**, *41*, 284–290.

(10) Israelachvili, J. N. *Intermolecular and surface forces*; 3rd Edition; Academic Press: Burlington, MA, 2011.

(11) Xiao, X.; Qian, L. Investigation of humidity-dependent capillary force. *Langmuir* **2000**, *16*, 8153–8158.

(12) Binnig, G.; Quate, C. F.; Gerber, C. Atomic force microscope. *Phys. Rev. Lett.* **1986**, *56*, 930−933.
(13) Larson, I.; Drummond, C. J.; Chan, D. Y. C.; Grieser, F. Direct force measurements between titanium dioxide surfaces. *J. Am. Chem. Soc.* **1993**, *115*, 11885−11890.
(14) Ong, Q. K.; Sokolov, I. Attachment of nanoparticles to the AFM tips for direct measurements of interaction between a single nanoparticle and surfaces. *J. Colloid Interface Sci.* **2007**, *310*, 385−390.
(15) Vakarelski, I. U.; Higashitani, K. Single-nanoparticle-terminated tips for scanning probe microscopy. *Langmuir* **2006**, *22*, 2931−2934.
(16) Volkov, D. O.; Dandu, P. R. V.; Goodman, H.; Santora, B.; Sokolov, I. Influence of adhesion of silica and ceria abrasive nanoparticles on chemical-mechanical planarization of silica surfaces. *Appl. Surf. Sci.* **2011**, *257*, 8518−8524.
(17) Rong; Ding, W.; Mädler, L.; Ruoff, R. S.; Friedlander, S. K. Mechanical properties of nanoparticle chain aggregates by combined AFM and SEM: Isolated aggregates and networks. *Nano Lett.* **2006**, *6*, 2646−2655.
(18) Rong, W.; Pelling, A. E.; Ryan, A.; Gimzewski, J. K.; Friedlander, S. K. Complementary TEM and AFM force spectroscopy to characterize the nanomechanical properties of nanoparticle chain aggregates. *Nano Lett.* **2004**, *4*, 2287−2292.
(19) Koparde, V. N.; Cummings, P. T. Phase Transformations during sintering of titania nanoparticles. *ACS Nano* **2008**, *2*, 1620−1624.
(20) Alimohammadi, M.; Fichthorn, K. A. Molecular dynamics simulation of the aggregation of titanium dioxide nanocrystals: preferential alignment. *Nano Lett.* **2009**, *9*, 4198−4203.
(21) Diebold, U. The surface science of titanium dioxide. *Surf. Sci. Rep.* **2003**, *48*, 53−229.
(22) Henderson, M. A. Structural sensitivity in the dissociation of water on TiO_2 single-crystal surfaces. *Langmuir* **1996**, *12*, 5093−5098.
(23) Mädler, L.; Kammler, H. K.; Mueller, R.; Pratsinis, S. E. Controlled synthesis of nanostructured particles by flame spray pyrolysis. *J. Aerosol Sci.* **2002**, *33*, 369−389.
(24) Mädler, L.; Roessler, A.; Pratsinis, S. E.; Sahm, T.; Gurlo, A.; Barsan, N.; Weimar, U. Direct formation of highly porous gas-sensing films by in situ thermophoretic deposition of flame-made Pt/SnO_2 nanoparticles. *Sens. Actuators* **2006**, *114*, 283−295.
(25) Birkenstock, J.; Fischer, R. X.; Messner, T. BRASS, the Bremen Rietveld analysis and structure suite. *Z. Kristallogr. Suppl.* **2006**, 237−242.
(26) Plimpton, S. Fast parallel algorithms for short-range molecular-dynamics. *J. Comput. Phys.* **1995**, *117*, 1−19.
(27) Schneider, J.; Ciacchi, L. C. First principles and classical modeling of the oxidized titanium (0001) surface. *Surf. Sci.* **2010**, *604*, 1105−1115.
(28) Matsui, M.; Akaogi, M. Molecular dynamics simulation of the structural and physical properties of the four polymorphs of TiO_2. *Mol. Simul.* **1991**, *6*, 239−244.
(29) Schneider, J.; Ciacchi, L. C. A Classical potential to model the adsorption of biological molecules on oxidized titanium surfaces. *J. Chem. Theory Comput.* **2011**, *7*, 473−484.
(30) Jorgensen, W. L.; Chandrasekhar, J.; Madura, J. D.; Impey, R. W.; Klein, M. L. comparison of simple potential functions for simulating liquid water. *J. Chem. Phys.* **1983**, *79*, 926−935.
(31) Rief, M.; Gautel, M.; Oesterhelt, F.; Fernandez, J. M.; Gaub, H. E. Reversible unfolding of individual titin immunoglobulin domains by AFM. *Science* **1997**, *276*, 1109−1112.
(32) Lausmaa, J.; Lofgren, P.; Kasemo, B. Adsorption and coadsorption of water and glycine on TiO_2. *J. Biomed. Mater. Res.* **1999**, *44*, 227−242.
(33) Fairbairn, E. A.; Keller, A. A.; Mädler, L.; Zhou, D.; Pokhrel, S.; Cherr, G. N. Metal oxide nanomaterials in seawater: Linking physicochemical characteristics with biological response in sea urchin development. *J. Hazard. Mater.* **2011**, *192*, 1565−1571.
(34) Ramirez-Garcia, S.; Chen, L.; Morris, M. A.; Dawson, K. A. A new methodology for studying nanoparticle interactions in biological systems: Dispersing titania in biocompatible media using chemical stabilisers. *Nanoscale* **2011**, *3*, 4617−4624.
(35) Warheit, D. B.; Webb, T. R.; Sayes, C. M.; Colvin, V. L.; Reed, K. L. Pulmonary instillation studies with nanoscale TiO_2 rods and dots in rats: Toxicity is not dependent upon particle size and surface area. *Toxicol. Sci.* **2006**, *91*, 227−236.
(36) Nel, A. E.; Madler, L.; Velegol, D.; Xia, T.; Hoek, E. M. V.; Somasundaran, P.; Klaessig, F.; Castranova, V.; Thompson, M. Understanding biophysicochemical interactions at the nano-bio interface. *Nat. Mater.* **2009**, *8*, 543−557.